

Ultra-low temperature sintering and temperature stable microwave dielectrics of $(\text{Mg}_{1-x}\text{Zn}_x)\text{V}_2\text{O}_6$ ($x=0-0.09$) Ceramics

Cheng-Liang Huang, Jyun-Lin Huang & Meng-Hung Tsai

To cite this article: Cheng-Liang Huang, Jyun-Lin Huang & Meng-Hung Tsai (2021) Ultra-low temperature sintering and temperature stable microwave dielectrics of $(\text{Mg}_{1-x}\text{Zn}_x)\text{V}_2\text{O}_6$ ($x=0-0.09$) Ceramics, Journal of Asian Ceramic Societies, 9:1, 106-112, DOI: [10.1080/21870764.2020.1848037](https://doi.org/10.1080/21870764.2020.1848037)

To link to this article: <https://doi.org/10.1080/21870764.2020.1848037>



© 2020 The Author(s). Published by Informa UK Limited, trading as Taylor & Francis Group on behalf of The Korean Ceramic Society and The Ceramic Society of Japan.



Published online: 15 Dec 2020.



Submit your article to this journal [↗](#)



Article views: 302




View related articles [↗](#)



View Crossmark data [↗](#)

Ultra-low temperature sintering and temperature stable microwave dielectrics of $(\text{Mg}_{1-x}\text{Zn}_x)\text{V}_2\text{O}_6$ ($x = 0\text{--}0.09$) Ceramics

Cheng-Liang Huang, Jyun-Lin Huang and Meng-Hung Tsai 

Department of Electrical Engineering, National Cheng Kung University, Tainan, Taiwan

ABSTRACT

Novel ultra-low firing $(\text{Mg}_{1-x}\text{Zn}_x)\text{V}_2\text{O}_6$ ($x = 0\text{--}0.09$) ceramics have been investigated and systematically designed as promising dielectrics for ultra-low temperature co-fired ceramics applications. The X-ray diffraction patterns indicated that all samples crystallized in a monoclinic structure with a space group of $\text{C}_{2/m}$. Microstructures and lattice parameters are presented and correlated with the microwave dielectric properties of the ceramics. The MgV_2O_6 specimen can be well-sintered at 610°C , the resulting ceramic of which featured an $\epsilon_r \sim 8.8$, a $Q \times f \sim 10,300$ GHz and a $\tau_f \sim -29.7$ ppm/ $^\circ\text{C}$. The tunable τ_f value can be adjusted to near zero along with a great promotion in the $Q \times f$ of MgV_2O_6 by using a small Zn substitution. In addition, excellent microwave dielectric properties ($\epsilon_r \sim 9.3$, $Q \times f \sim 15,300$ GHz @15.5 GHz and $\tau_f \sim -3.4$ ppm/ $^\circ\text{C}$) were obtained for the $(\text{Mg}_{0.93}\text{Zn}_{0.07})\text{V}_2\text{O}_6$ specimen sintered at 610°C for 4 h. The specimen is chemically compatible with Al electrodes and could be an ideal ultra-low temperature co-fired ceramics dielectric. Possible applications include the 5 G system, particularly with high frequency regions.

ARTICLE HISTORY

Received 23 August 2020
Accepted 5 November 2020

KEYWORDS

ULTCC; $(\text{Mg}_{1-x}\text{Zn}_x)\text{V}_2\text{O}_6$ ceramics; High-Q; microwave dielectric properties; 5G

1. Introduction

With the progress of today's wireless communication systems, the requirement of Low Temperature Co-fired Ceramics (LTCC) technology to miniaturize and integrate microwave passive components and devices is more needed than ever. Major requisites for LTCC dielectrics include a low dielectric constant ($\epsilon_r < 10$) to reduce the wave propagation delay of the system, a high $Q \times f$ value to lower the dielectric loss at high frequency operation, and a near-zero temperature coefficient of resonant frequency (τ_f) to limit the resonator frequency shift. For energy conservation, Al (melting point at 660°C) is normally preferred and selected as the electrode material for Ultra-Low Temperature Co-firing Ceramics (ULTCC) applications. Consequently, a $< 660^\circ\text{C}$ sintering temperature is required for the dielectrics to prevent the electrode from melting. To this end, glass addition and sol-gel processing are usually employed to reduce the sintering temperature of dielectric ceramics. However, glass-added sintering also degrades the microwave dielectric properties of ceramics. Moreover, a costly, time-consuming, and complex processing is required for the sol-gel method. Most of the ULTCC reveal a negative τ_f value [1–3]. To compensate the negative τ_f value, dielectrics with a positive τ_f , which also means a high ϵ_r and a low $Q \times f$, are often added to the ceramics, resulting in the combined microwave dielectric properties also being distorted, thereby limiting possible applications at high frequency regimes, such as a 5G system [4,5]. For instance,

high ϵ_r (> 10) dielectrics increase the wave propagation delay of devices for high frequency applications. Therefore, the search for new dielectrics, particularly with a stable τ_f for ULTCC applications has become a more urgent issue.

A number of V_2O_5 -based ceramic families have been studied and reported for LTCC applications over the last decade. For instance, BaV_2O_6 and $\text{Ba}_3\text{V}_4\text{O}_{13}$, belonging to the $\text{BaO-V}_2\text{O}_5$ family, have been reported to be good candidates for ULTCC applications [6,7]. The $\text{R}_2\text{V}_2\text{O}_7$ ($\text{R} = \text{Ba}, \text{Sr}$ and Ca), $\text{BaO-MO-V}_2\text{O}_5$ ($\text{M} = \text{Mg}, \text{Zn}$), and SrMV_2O_7 ($\text{M} = \text{Mg}, \text{Zn}$) families have also been found to offer good microwave dielectric properties at ultra-low sintering temperatures [8,9]. Moreover, $\text{Mg}_3(\text{VO}_4)_2$ and $\text{BaMg}_2(\text{VO}_4)_2$ have been proposed as suitable LTCC dielectrics [10–12]. Nevertheless, they possess a large negative τ_f , which limits their practical applications.

In this paper, a novel ULTCC $(\text{Mg}_{1-x}\text{Zn}_x)\text{V}_2\text{O}_6$ ($x = 0\text{--}0.09$) dielectric with a near-zero τ_f was investigated. In doing so, the X-ray Diffraction (XRD) patterns and surface morphology were studied. Additionally, the compatibility of co-firing with an Al electrode was also reported.

2. Materials and methods

V_2O_5 , MgO , and ZnO powders ($> 99.9\%$) were mixed according to the $(\text{Mg}_{1-x}\text{Zn}_x)\text{V}_2\text{O}_6$ ($x = 0\text{--}0.09$) composition. The powders were ball-milled for 24 h, dried and calcined at 500°C for 2 h. The mixtures, together with PVA binder, were subsequently granulated and uniaxially pressed into pellets with 5 mm in thickness and

11 mm in diameter at 2000 kg/cm^2 . All samples were then sintered at $520\text{--}640^\circ\text{C}$ for 4 h. The subsequent phase identification of the specimens was conducted by XRD pattern analysis using a Siemens D5000 diffractometer (Munich, Germany) with Cu-K α radiation (at 40kV and 40 mA). Thermal Gravity-Differential Scanning Calorimetry (TG-DSC) analyses (NETZSCH STA409PC) were employed in analyzing the phase formation of the samples. The microstructures and the compatibility of co-firing with Al were studied using ultra-high resolution scanning electron microscopy (UHR-SEM; HitachiSU-8000) equipped with energy dispersion spectroscopy (EDS, Philips). The Archimedes method was applied to measure the densities of the specimens. Dielectric constants and $Q \times f$ values of the samples were measured using the Hakki-Coleman [13] and Courtney [14] methods on an Agilent 8364A network analyzer (USA). The same technique was applied to measure the τ_f value and can be expressed by

$$\tau_f = (f_2 - f_1) / [f_1(T_2 - T_1)] \quad (1)$$

Where f_1 and f_2 represent the resonant frequencies at T_1 and T_2 , respectively. All specimens were measured at $25\text{--}80^\circ\text{C}$. Rietveld refinement was completed by using the General Structure and Analysis System(GSAS).

3. Results and discussion

Figure 1 illustrates the TG-DSC curves of the MgV_2O_6 precursor powders performed by the thermal analyzer. There are two mass losses of the ceramic, the first of which constitutes a total weight loss of 3.7% occurring before reaching 258°C , and the second major weight loss of 10.2% observed during the second stage from 258°C to 450°C . Further increases in the temperature led to no additional obvious weight losses, suggesting that the formation of the MgV_2O_6 phase was complete. According to the DSC curve, the small endothermic peak appearing at 185°C was most likely caused by free-water evaporation. The second endothermic peak occurring at 245°C along with weight loss was due to the evaporation of crystal water or the

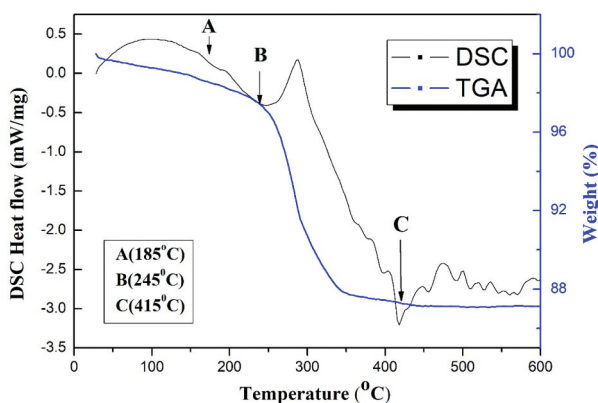


Figure 1. TG-DSC curves of MgV_2O_6 ceramics.

decomposition of $\text{Mg}(\text{OH})_2$. In addition, an endothermic peak appearing at 415°C was due to the formation of the MgV_2O_6 phase at the final stage. As can be seen, there are some exothermic peaks observed between 450 and 550°C corresponding to the heat-release process of adjusting the lattice structure in the late stage of the reaction. Based upon the TG-DSC curves, the calcination temperature of the MgV_2O_6 precursor powders was then chosen to range from $450\text{--}550^\circ\text{C}$.

The XRD patterns of the $(\text{Mg}_{1-x}\text{Zn}_x)\text{V}_2\text{O}_6$ ($x = 0\text{--}0.09$) ceramics recorded at room temperature are shown in Figure 2. The specimens exhibited a monoclinic structure with a space group of $C_{2/m}$ [11] in accordance with the standard ICDD-PDF #01-071-1651. Additionally, no second phase was detected in all cases, suggesting the formation of a solid solution. With an increase in x , peaks shifted to a lower angle due to the replacement of Mg^{2+} (0.72 \AA , CN = 6) by the larger Zn^{2+} (0.74 \AA , CN = 6). In addition, no peak shift was observed for the $(\text{Mg}_{0.93}\text{Zn}_{0.07})\text{V}_2\text{O}_6$ specimen at various temperatures, indicating that the influence of the sintering temperature on structure could be excluded. However, the full width at half maximum (FWHM) decreased as the sintering temperature increased, which implies better crystallinity. In order to further clarify the crystal structure of the $(\text{Mg}_{1-x}\text{Zn}_x)\text{V}_2\text{O}_6$ ($x = 0\text{--}0.09$) ceramics, GSAS software was used to conduct Rietveld refinements. Table 1 illustrates the resultant refined lattice parameters, molecular volume, reliability factors, and goodness of fit indicators. As seen, the variations of lattice parameters and cell volumes were limited and within 1%, and the goodness of fit indicator values (χ^2) were in the range 0.98–1.28, which suggests that the structural model is valid along with

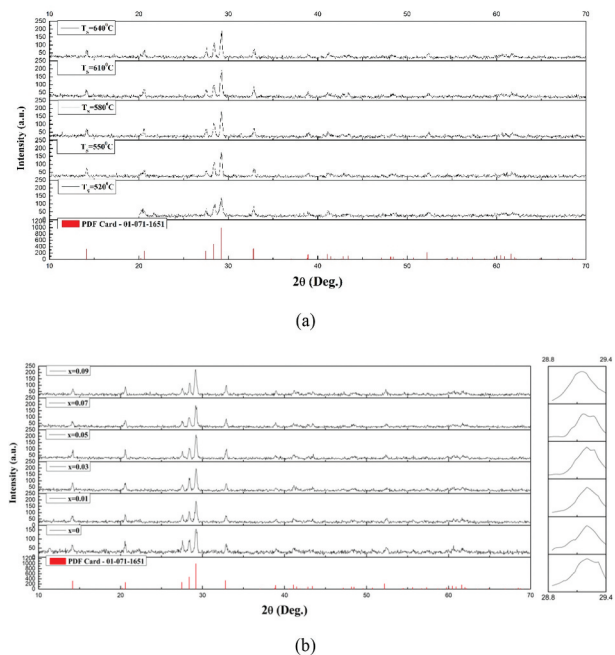


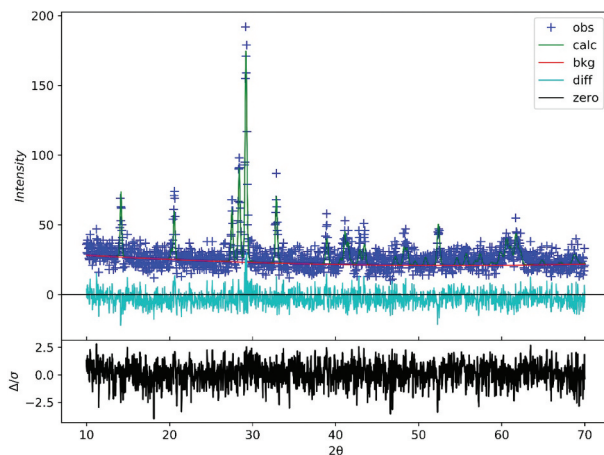
Figure 2. Room temperature XRD patterns recorded from $(\text{Mg}_{1-x}\text{Zn}_x)\text{V}_2\text{O}_6$ ceramics with (a) $x = 0.07$ at different temperatures and (b) $x = 0\text{--}0.09$ at 610°C .

Table 1. The refined lattice parameters, molecular volume, goodness of fit, and reliability factors, of the $(\text{Mg}_{1-x}\text{Zn}_x)\text{V}_2\text{O}_6$ ceramics sintered at 610°C.

x content	x = 0	x = 0.01	x = 0.03	x = 0.05	x = 0.07	x = 0.09
a	9.29023	9.29019	9.29119	9.29463	9.29048	9.29328
b	3.48903	3.48252	3.46372	3.47842	3.49837	3.50028
c	6.71728	6.71389	6.70429	6.71229	6.72606	6.72853
Cell Volume (\AA^3)	202.114	202.737	201.376	201.528	202.937	203.601
$R_{wp}(\%)$	20.298	19.065	19.214	18.064	19.76	19.94
χ^2	1.28	1.1	1.08	0.98	1.08	1.1
ϵ_r	8.8	8.1	8.8	9	9.3	8.7
ϵ_{rc}	9.9	9.3	9.9	9.7	10	9.5
$V_m(\text{\AA}^3)$	101.057	101.369	100.688	100.764	101.469	101.801
$a_D(\text{\AA}^3)$	18.04	17.78	17.98	17.88	18.17	17.96

reliable refinement results. Moreover, the refined plot of the specimen using $(\text{Mg}_{0.93}\text{Zn}_{0.07})\text{V}_2\text{O}_6$ at 610°C is illustrated in Figure 3, which shows that the identical results were obtained as those in Table 1. These results also confirmed the formation of a single monoclinic structure phase.

The surface micro-morphology of the $(\text{Mg}_{1-x}\text{Zn}_x)\text{V}_2\text{O}_6$ ($x = 0-0.09$) ceramics is presented in Figure 4. A porous microstructure was observed for the $(\text{Mg}_{0.93}\text{Zn}_{0.07})\text{V}_2\text{O}_6$ ceramic specimen at 520°C. As the sintering temperature was increased, the number of pores decreased and a well-densified morphology was achieved at 610°C. In addition, rapid grain growth occurred at 640°C, indicating an over-sintering temperature for the specimen. Obviously, the grains exhibited a typical polygonal morphology for all specimens. Large grains and small grains co-existed, with both corresponding to a single MgV_2O_6 phase, as further confirmed by the EDS results (Table 2). Moreover, specimens with $x = 0$ and 0.01 showed rough grain boundaries, which were improved as x was increased, with smooth grain boundaries being observed for $x > 0.03$, suggesting Zn may aid the sintering process. In addition, the specimen with $x = 0.09$ was found to have an obviously larger grain size and a less uniform morphology compared to that of $x = 0.07$, which may have negative effects on the $Q \times f$ values of the specimen.

**Figure 3.** Refined plot of the specimen using $(\text{Mg}_{0.93}\text{Zn}_{0.07})\text{V}_2\text{O}_6$ at 610°C.

The relative densities of the monoclinic $(\text{Mg}_{1-x}\text{Zn}_x)\text{V}_2\text{O}_6$ ($x = 0-0.09$) ceramics sintered at different temperatures are demonstrated in Figure 5. The low relative density of 87%–91% observed for specimens sintered at 520°C was most likely a result of the porous morphology, as shown in Figure 3. However, the density initially increased with increases in sintering temperature, and then decreased after reaching a maximum at 610°C. In all cases, the optimal sintering temperature was 610°C. A high relative density of 95.3% was obtained for the specimen with $x = 0.07$ sintered at 610°C.

Figure 6 illustrates the plots of ϵ_r as a function of temperature for the $(\text{Mg}_{1-x}\text{Zn}_x)\text{V}_2\text{O}_6$ ($x = 0-0.09$) ceramics. The variations in ϵ_r were consistent with those of the relative density, indicating that density might be a primary factor affecting ϵ_r in this experiment. Moreover, a maximum ϵ_r value of ~ 9.3 was achieved corresponding to the highest relative density of 95.3% for the $x = 0.07$ specimen sintered at 610°C. Shannon reported that ϵ_r is proportional to the a_D , and can be expressed by the Clausius–Mosotti equation [15]:

$$a_D = [V_m(\epsilon_{rc} - 1)]/[b(\epsilon_{rc} + 2)] \quad (2)$$

where V_m is the molecular volume, ϵ_{rc} represents the corrected dielectric constant, and the constant value $b = 4\pi/3$. According to Eqn. (2), ϵ_{rc} increases when a_D increases. As shown in Table 1, the variation of ϵ_{rc} is inversely proportional to that of V_m for $x = 0-0.05$, which is because the amount of Zn substitution is small. However, the change in ϵ_{rc} becomes consistent with that of a_D at $x = 0.07-0.09$ due to the fact that Zn^{2+} (1.7\AA^3) has a larger polarizability than Mg^{2+} (0.651\AA^3), which dominates the variation of ϵ_r in $(\text{Mg}_{1-x}\text{Zn}_x)\text{V}_2\text{O}_6$ ceramics.

Figure 7 demonstrates the $Q \times f$ values of the $(\text{Mg}_{1-x}\text{Zn}_x)\text{V}_2\text{O}_6$ ($x = 0-0.09$) ceramics sintered at various temperatures. Both intrinsic and extrinsic losses are included in the overall measured microwave dielectric losses. Typical intrinsic loss is mainly a result of the lattice vibration modes; extrinsic loss, however, can be related to density, second phases, impurities, surface morphology, and the lattice defects [16,17]. Accordingly, the $Q \times f$ increased with increases in sintering temperature, reaching a maximum at 610°C, which corresponds to the

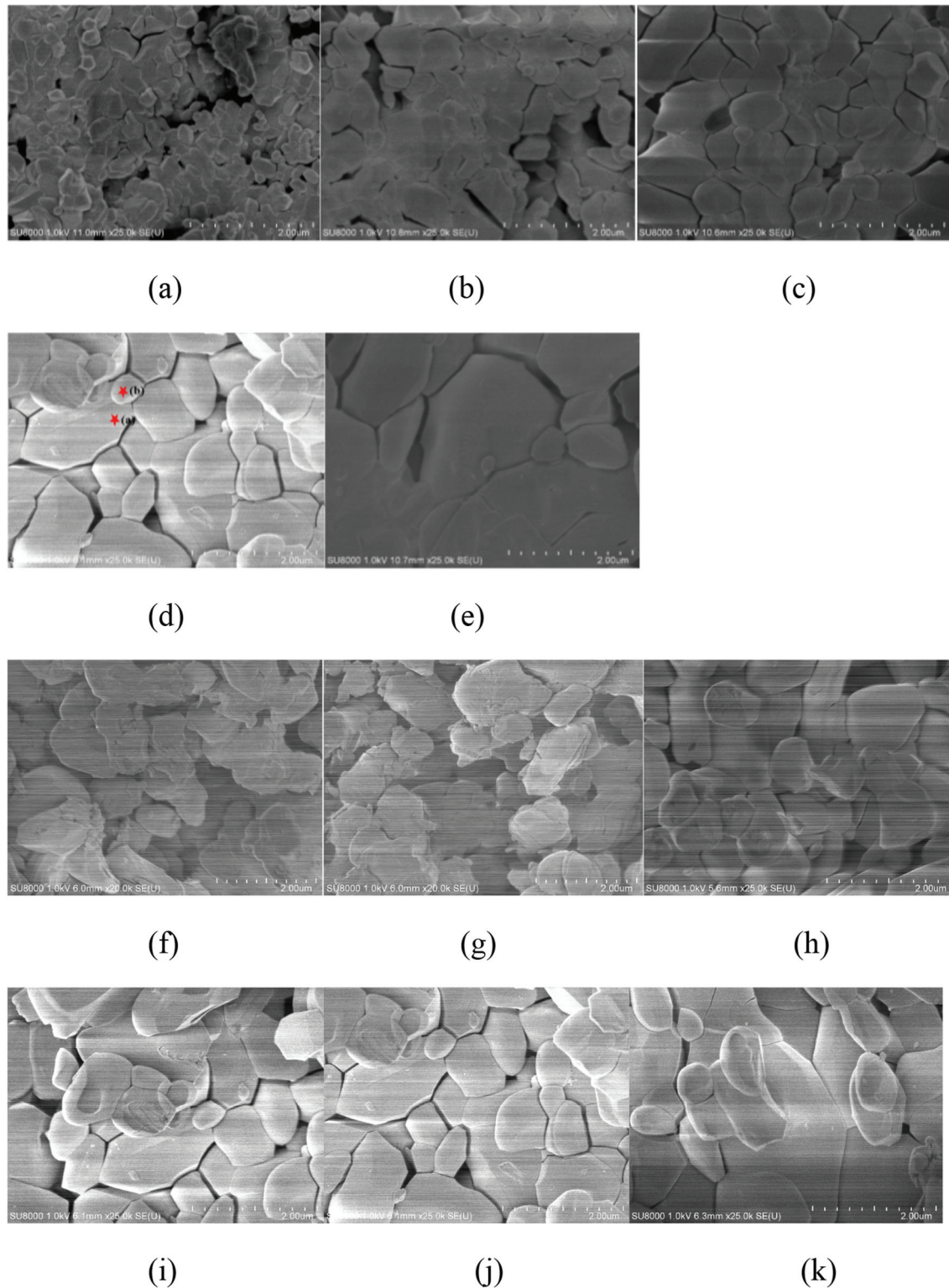


Figure 4. SEM images of $(\text{Mg}_{1-x}\text{Zn}_x)\text{V}_2\text{O}_6$ sintered at (a) 520°C (b) 550°C (c) 580°C (d) 610°C (e) 640°C and of $(\text{Mg}_{1-x}\text{Zn}_x)\text{V}_2\text{O}_6$ with (f) $x = 0$ (g) $x = 0.01$ (h) $x = 0.03$ (i) $x = 0.05$ (j) $x = 0.07$ (k) $x = 0.09$ sintered at 610°C.

Table 2. Corresponding EDS results of Figure 4(d).

	Spot a				Spot b			
	Mg K	Zn K	V L	O K	Mg K	Zn K	V L	O K
Weight%	10.14	2.13	44.02	43.71	10.02	2.01	45.11	42.86
Atomic%	10.55	0.82	21.61	68.33	10.43	0.78	22.15	67.00

optimal sintering temperature mentioned earlier, and decreased thereafter. Moreover, the variations of $Q \times f$ for specimens with $x = 0$ –0.09 at 610°C was

also consistent with those of the relative density, implying that the dielectric loss of specimens was mainly attributed to the extrinsic loss corresponding to the densification of ceramics. Compared to the $x = 0$ specimen, the $x = 0.07$ specimen exhibited a 50% increase in the $Q \times f$ and a maximum value of 15,300 GHz @15.5 GHz could be achieved for the $(\text{Mg}_{0.93}\text{Zn}_{0.07})\text{V}_2\text{O}_6$ specimen sintered at 610°C.

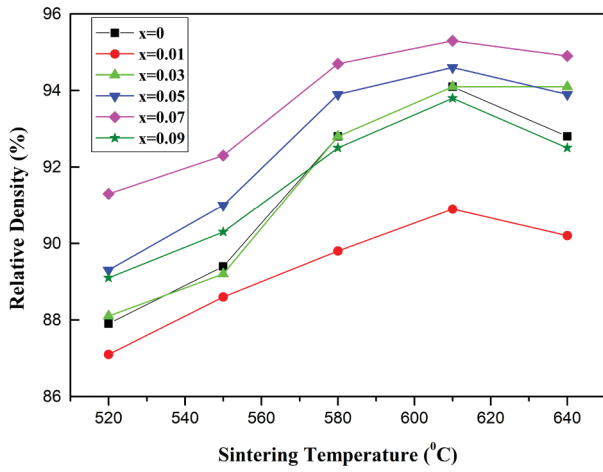


Figure 5. Relative densities of the $(\text{Mg}_{1-x}\text{Zn}_x)\text{V}_2\text{O}_6$ ($x = 0-0.09$) ceramics at different sintering temperatures.

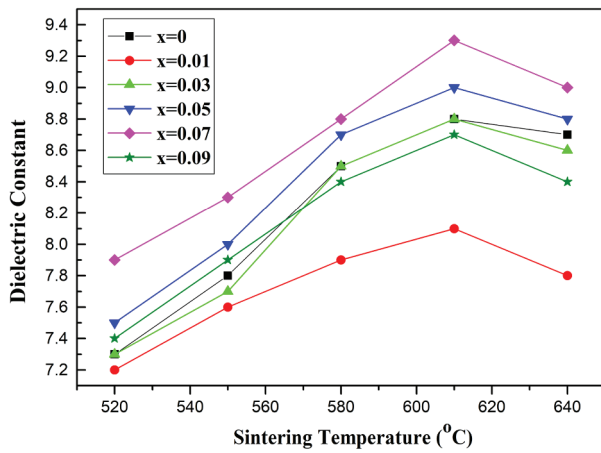


Figure 6. ϵ_r values of the $(\text{Mg}_{1-x}\text{Zn}_x)\text{V}_2\text{O}_6$ ($x = 0-0.09$) ceramics at different sintering temperatures.

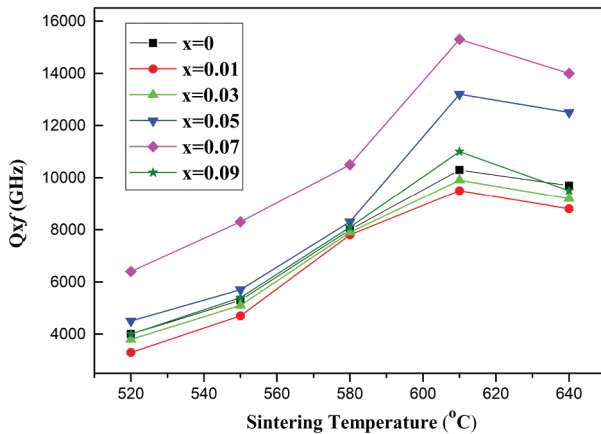


Figure 7. $Q \times f$ values of the $(\text{Mg}_{1-x}\text{Zn}_x)\text{V}_2\text{O}_6$ ($x = 0-0.09$) ceramics at different sintering temperatures.

Figure 8 illustrates τ_f values of the $(\text{Mg}_{1-x}\text{Zn}_x)\text{V}_2\text{O}_6$ ($x = 0-0.09$) ceramics sintered at different temperatures. Since there is no second phase in the pure monoclinic specimen, the remarkable shift of their values from -38.7 to -3.64 ppm/°C in the $(\text{Mg}_{1-x}\text{Zn}_x)\text{V}_2\text{O}_6$ ($x = 0-0.09$) ceramics was mainly attributable

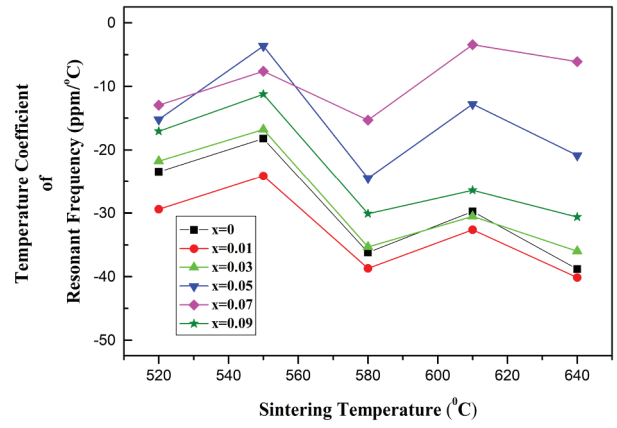


Figure 8. τ_f values of the $(\text{Mg}_{1-x}\text{Zn}_x)\text{V}_2\text{O}_6$ ($x = 0-0.09$) ceramics at different sintering temperatures.

to the Zn^{2+} substitution for Mg^{2+} . By tuning the x to 0.07, the specimen had a τ_f of -3.64 ppm/°C at 610°C .

The microwave dielectric properties and sintering temperatures of some typical ceramics for ULTCC applications are listed in Table 3. All the dielectrics can be co-fired with aluminum. However, the first four compositions reveal a large τ_f value that limits their practical applications. In the next two ceramics, the τ_f was modified to a near-zero value; yet, it still suffers from a high ϵ_r , constraining its high frequency applications. In addition, tellurium oxide is toxic and not preferred for use in components. In comparison, the proposed $(\text{Mg}_{0.93}\text{Zn}_{0.07})\text{V}_2\text{O}_6$ specimen not only has a near-zero τ_f it also exhibits a moderate $Q \times f$ and a low ϵ_r , making it a very promising dielectric for ULTCC applications, particularly for the high frequency 5G system.

For ULTCC applications, Figure 9 illustrates the EDS line scan and corresponding SEM photo of the interface between the Al electrode and the $(\text{Mg}_{0.93}\text{Zn}_{0.07})\text{V}_2\text{O}_6$ specimen co-fired at 610°C . As seen, a sharp decrease in the Al profile at the interface implies that Al did not diffuse into the ceramic during co-firing. Moreover, a very low amount of Mg and V in the Al electrode also suggests that no reaction occurred at the interface. Since the specimen revealed a chemical compatibility with Al, it is

Table 3. Microwave dielectric properties and sintering temperatures of some typical ceramics for ULTCC applications.

Composition	S.T. (°C)	f_r (GHz)	ϵ_r	$Q \times f$ (GHz)	τ_f (ppm/°C)	Ref.
Ag_2MoO_4	450	—	8.1	17,000	-133	[1]
$\text{Ag}_2\text{Mo}_2\text{O}_7$	460	9.25	13.3	25,300	-142	[2]
$\text{Ag}_6\text{Mo}_{10}\text{O}_{33}$	500	9	14	8,500	-50	[2]
$\text{Na}_2\text{Zn}_5(\text{MoO}_4)_6$	590	—	8.1	35,800	-95	[3]
$0.25\text{Na}_2\text{Mo}_2\text{O}_7$	580	6.2	24	13,000	3	[4]
$-0.75\text{Na}_{0.5}\text{Bi}_{0.5}\text{MoO}_4$						
BaTe_4O_9	575	—	25	19,300	-3	[5]
+ 40 wt% TiTe_3O_8						
$(\text{Mg}_{0.93}\text{Zn}_{0.07})\text{V}_2\text{O}_6$	610	15.5	9.3	15,300	-3.4	This work

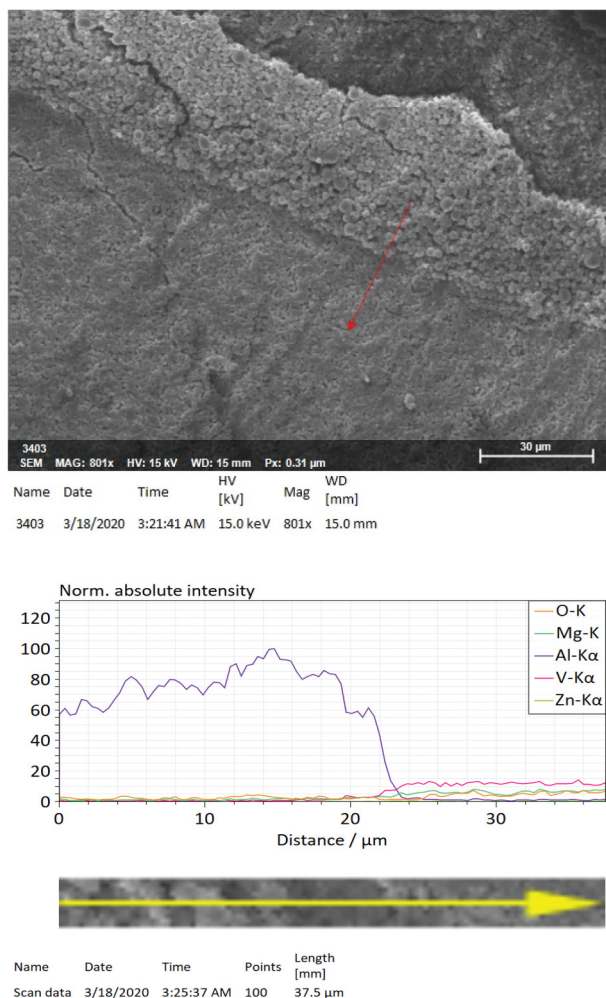


Figure 9. SEM image and EDS line scan of the $(\text{Mg}_{0.93}\text{Zn}_{0.07})\text{V}_2\text{O}_6$ specimen co-fired with Al electrode at 610°C .

further confirmed as an ideal candidate dielectric for ULTCC applications.

4. Conclusion

The $(\text{Mg}_{1-x}\text{Zn}_x)\text{V}_2\text{O}_6$ ($x = 0-0.09$) ceramics were prepared via the conventional solid-state route. Specimens sintered at $520-640^\circ\text{C}$ for 4 h exhibited a monoclinic structure with a space group of $\text{C}_{2/m}$ without evidence of any additional second phase, suggesting the formation of a solid solution. The microwave dielectric properties were correlated to the microstructures, the temperatures, and the relative densities of the ceramics. The $(\text{Mg}_{0.93}\text{Zn}_{0.07})\text{V}_2\text{O}_6$ ceramic reveals an ϵ_r of 9.3, a $Q \times f$ of 15,300 GHz and a τ_f of $-3.4 \text{ ppm}/^\circ\text{C}$. The EDS line scan of the $(\text{Mg}_{0.93}\text{Zn}_{0.07})\text{V}_2\text{O}_6$ sample co-fired with aluminum also shows an excellent chemical compatibility and is presented as an ideal candidate dielectric for ULTCC applications.

Acknowledgments

The work was financially sponsored by the Ministry of Science and Technology of Taiwan under the projects

MOST 109-2221-E-006-139. The authors gratefully acknowledge the use of D8 Discover equipment belonging to the Instrument Center of National Cheng Kung University.

Disclosure statement

The authors declare that they have no known competing financial interests or personal relationships that could have appeared to influence the work reported in this paper.

Funding

This work was supported by the Ministry of Science and Technology, Taiwan [MOST 109-2221-E-006-139].

ORCID

Meng-Hung Tsai  <http://orcid.org/0000-0002-7917-0728>

References

- [1] Zhou D, Li WB, Pang LX, et al. Sintering behavior and dielectric properties of ultra-low temperature fired silver molybdate ceramics. *J Am Ceram Soc.* **2014** Nov;97(11):3597–3601.
- [2] Dhanya J, Basiluddeen AV, Ratheesh R. Synthesis of ultra low temperature sinterable $\text{Na}_2\text{Zn}_5(\text{MoO}_4)_6$ ceramics and the effect of microstructure on microwave dielectric properties. *Scripta Mater.* **2017** Apr 15;132:1–4.
- [3] Zhang GQ, Guo J, Wang H. Ultra-low temperature sintering microwave dielectric ceramics based on $\text{Ag}_2\text{O}-\text{MoO}_3$ binary system. *J Am Ceram Soc.* **2017** Jun;100(6):2604–2611.
- [4] Jiao XQ, Zhong CW, Zhang SR, et al. Microwave dielectric properties of $\text{BaO}-\text{TiO}_2-\text{TeO}_2$ ternary system. *J Mater Sci.* **2010** Jun;45(12):3331–3335.
- [5] Zhang GQ, Guo J, Yuan XF, et al. Ultra-low temperature sintering and microwave dielectric properties of a novel temperature stable $\text{Na}_2\text{Mo}_2\text{O}_7-\text{Na}_0.5\text{Bi}_0.5\text{MoO}_4$ ceramic. *J Eur Ceram Soc.* **2018** Feb;38(2):813–816.
- [6] Neelakantan UA, Kalathil SE, Ratheesh R. Structure and microwave dielectric properties of ultralow-temperature cofirable BaV_2O_6 ceramics. *Eur J Inorg Chem.* **2015** Jan;(2):305–310. DOI:10.1002/ejic.201402844.
- [7] Kalathil SE, Neelakantan UA, Ratheesh R. Microwave dielectric properties of ultralow-temperature cofirable $\text{Ba}_3\text{V}_4\text{O}_{13}$ ceramics. *J Am Ceram Soc.* **2014** May;97(5):1530–1533.
- [8] Joung MR, Kim JS, Song ME, et al. Formation process and microwave dielectric properties of the $\text{R}_2\text{V}_2\text{O}_7$ ($\text{R}=\text{Ba}$, Sr , and Ca) ceramics. *J Am Ceram Soc.* **2009** Dec;92(12):3092–3094.
- [9] Suresh EK, Ratheesh R. Structure and microwave dielectric properties of glass free low temperature co-firable SrMV_2O_7 ($\text{M} = \text{Mg}$, Zn) ceramics. *J Alloy Compd.* **2019** Nov 5;808. DOI: 10.1016/j.jallcom.2019.07.353.
- [10] Umemura R, Ogawa H, Ohsato H, et al. Microwave dielectric properties of low-temperature sintered $\text{Mg}-3(\text{VO}_4)(2)$ ceramic. *J Eur Ceram Soc.* **2005**;25(12):2865–2870.

- [11] Umemura R, Ogawa H, Kan A. Low temperature sintering and microwave dielectric properties of $(\text{Mg}_{3-x}\text{Zn}_x)(\text{VO}_4)_2$ ceramics. *J Eur Ceram Soc.* 2006;26 (10–11):2063–2068.
- [12] Umemura R, Ogawa H, Yokoi A, et al. Low-temperature sintering-microwave dielectric property relations in $\text{Ba}_3(\text{VO}_4)_2$ ceramic. *J Alloy Compd.* 2006 Nov 9;424 (1–2):388–393.
- [13] Hakki BW, Coleman PD, Dielectric Resonator A. Method of measuring inductive capacities in the millimeter range. *IRE Trans Microw Theory Tech.* 1960;8 (4):402–410.
- [14] Courtney WE. Analysis and evaluation of a method of measuring the complex permittivity and permeability microwave insulators. *IEEE Trans Microw Theory Tech.* 1970;18(8):476–485.
- [15] Shannon RD. Dielectric polarizabilities of ions in oxides and fluorides. *J Appl Phys.* 1993;73(1):348–366.
- [16] Silverman BD. Microwave absorption in cubic strontium titanate. *Phys Rev.* 1962;125(6):1921–1930.
- [17] Penn SJ, Alford NM, Templeton A, et al. Effect of porosity and grain size on the microwave dielectric properties of sintered alumina. *J Am Ceram Soc.* 1997;80 (7):1885–1888.